

Table of Contents: TCC News No. 68

El Niño Outlook (June - December 2022)	1
JMA's Seasonal Numerical Ensemble Prediction for Boreal Summer 2022	4
Summary of the 2021/2022 Asian Winter Monsoon	7
TCC and WMC Tokyo co-contributions to Regional Climate Outlook Forums	13

El Niño Outlook (June - December 2022)

Atmospheric and oceanic indicators suggest ongoing La Niña conditions in the equatorial Pacific. La Niña conditions are likely to continue until early boreal summer (70%). It is more likely to transfer to ENSO-neutral (60%) by the end of summer than to continue (40%) until boreal autumn (article based on the El Niño outlook issued on 10 June 2022).

1. El Niño/La Niña

In May 2022, the sea surface temperature (SST) for the NINO.3 region was below normal with a deviation of -1.0°C. Equatorial Pacific SSTs were below normal in central to eastern parts (Figures 1-1 and 1-3 (a)). Subsurface temperatures were above normal in the western part and below normal in the eastern part (Figures 1-2 and 1-3 (b)). Atmospheric convective activity near the date line over the equatorial Pacific was suppressed compared to the normal, and easterly winds in the lower troposphere (i.e., trade winds) over the central equatorial Pacific were stronger than normal. These oceanic and atmospheric conditions are consistent with features commonly seen in past La Niña events, and indicate that La Niña conditions remain ongoing in the equatorial Pacific.

Subsurface warm waters observed in the western equatorial Pacific are expected to migrate eastward and slightly increase SSTs in the eastern part in boreal summer. JMA's seasonal Ensemble Prediction System suggests that NINO.3 SSTs will slightly increase in boreal summer and remain around -0.5°C until boreal autumn (Figure 1-4). In conclusion, La Niña conditions are likely to continue (70%) until early boreal summer. However, it is more likely to transfer to ENSO-neutral (60%) by the end of summer than to continue (40%) until boreal autumn (Figure 1-5).

2. Western Pacific and Indian Ocean

The area-averaged SST in the tropical western Pacific (NINO.WEST) region was below normal in May. Index values are likely to be near or below normal until boreal autumn.

The area-averaged SST in the tropical Indian Ocean (IOBW) region was below normal in May. Index values are likely to be near or below normal until boreal autumn.

(SATO Hitoshi, Tokyo Climate Center)

* The SST normal for the NINO.3 region (5°S – 5°N, 150°W – 90°W) is defined as a monthly average over the latest sliding 30-year period (1992-2021 for this year).

* The SST normals for the NINO.WEST region (Eq. – 15°N, 130°E – 150°E) and the IOBW region (20°S – 20°N, 40°E – 100°E) are defined as linear extrapolations with respect to the latest sliding 30-year period, in order to remove the effects of significant long-term warming trends observed in these regions.

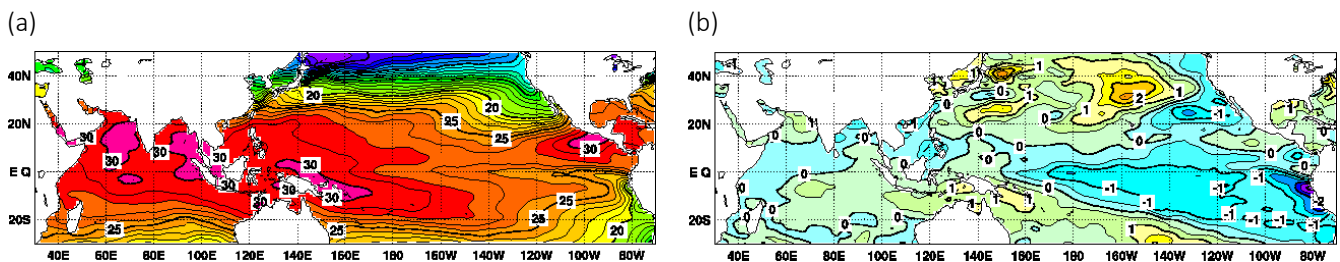


Figure 1-1 Monthly mean (a) sea surface temperatures (SSTs) and (b) SST anomalies in the Indian and Pacific Ocean areas for May 2022. The contour intervals are 1°C in (a) and 0.5°C in (b). The base period for the normal is 1991 – 2020.

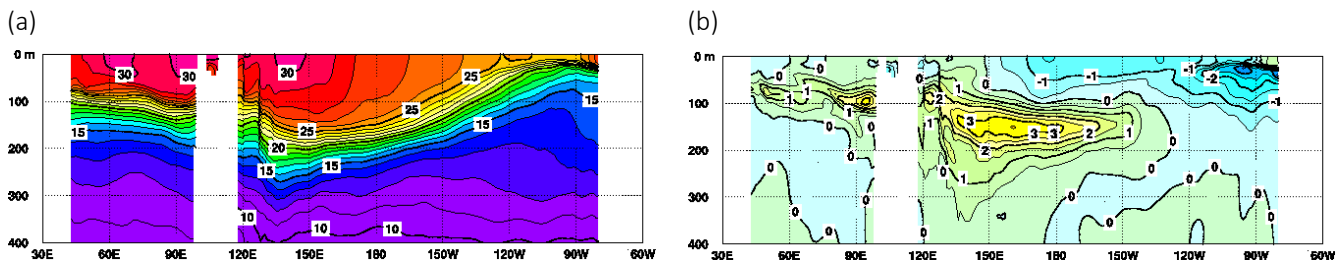


Figure 1-2 Monthly mean depth-longitude cross sections of (a) temperatures and (b) temperature anomalies in the equatorial Indian and Pacific Ocean areas for May 2022. The contour intervals are 1°C in (a) and 0.5°C in (b). The base period for the normal is 1991 – 2020.

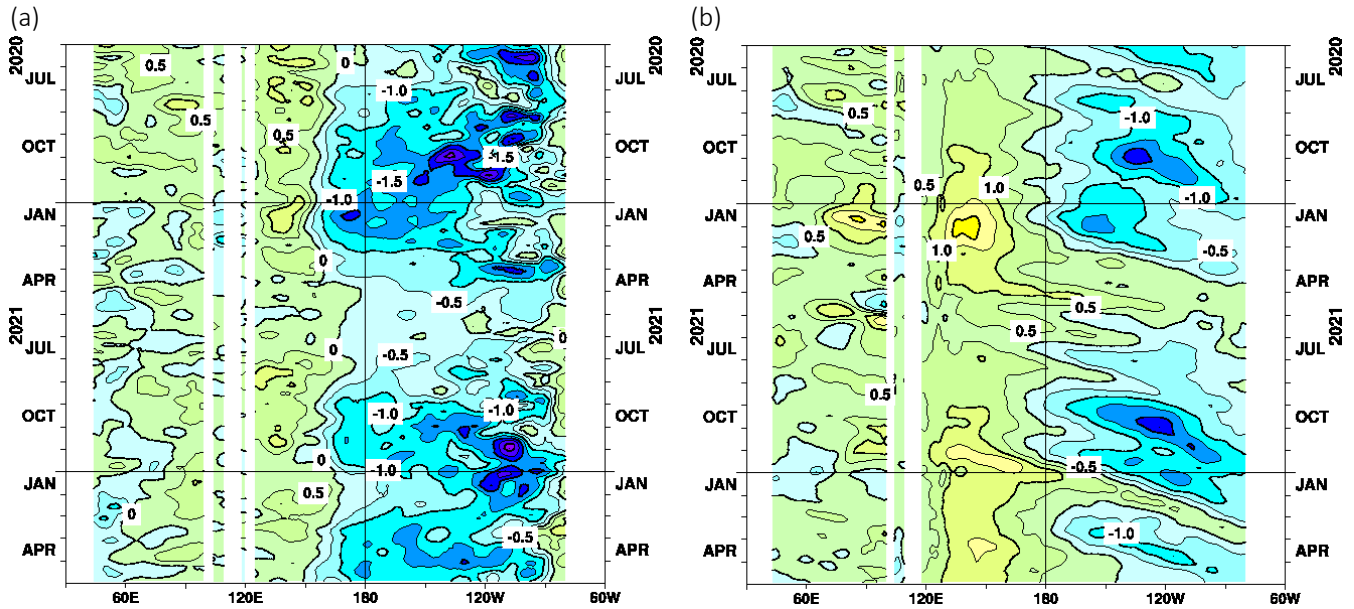


Figure 1-3 Time-longitude cross sections of (a) SST and (b) ocean heat content (OHC) anomalies along the equator in the Indian and Pacific Ocean areas

OHCs are defined here as vertically averaged temperatures in the top 300 m. The base period for the normal is 1991 – 2020.

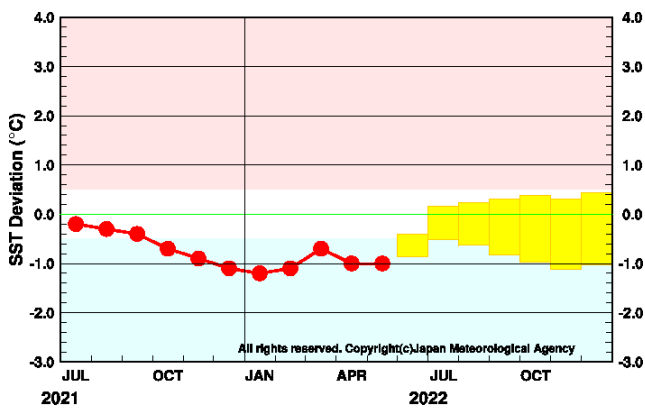


Figure 1-4 Outlook of NINO.3 SST deviation produced by the seasonal Ensemble Prediction System

This figure shows a time series of monthly NINO.3 SST deviations. The thick line with closed circles shows observed SST deviations, and the boxes show the values produced for up to six months ahead by the El Niño prediction model. Each box denotes the range into which the SST deviation is expected to fall with a probability of 70%.

YEAR	MONTH	mean period	El Niño	ENSO neutral	La Niña
2022	APR	FEB2022–JUN2022	100		
	MAY	MAR2022–JUL2022	20	80	
	JUN	APR2022–AUG2022	30	70	
	JUL	MAY2022–SEP2022	50	50	
	AUG	JUN2022–OCT2022	60	40	
	SEP	JUL2022–NOV2022	60	40	
	OCT	AUG2022–DEC2022	60	40	

Figure 1-5 ENSO forecast probabilities based on the seasonal Ensemble Prediction System

Red, yellow and blue bars indicate probabilities that the five-month running mean of the NINO.3 SST deviation from the latest sliding 30-year mean will be $+0.5^{\circ}\text{C}$ or above (El Niño), between $+0.4$ and -0.4°C (ENSO-neutral) and -0.5°C or below (La Niña), respectively. Regular text indicates past months, and bold text indicates current and future months.

[<<Table of contents](#) [<Top of this article](#)

JMA's Seasonal Numerical Ensemble Prediction for Boreal Summer 2022

This report outlines JMA’s dynamical seasonal ensemble prediction for boreal summer 2022 (June – August, referred to as JJA), which was used as a basis for JMA’s operational three-month outlook issued on 24 May 2022. The outlook is based on the seasonal ensemble prediction system of the Coupled Atmosphere-ocean General Circulation Model (CGCM).

Summary: Based on JMA’s seasonal ensemble prediction system, La Niña conditions are likely to continue until early boreal summer. In association with above-normal SSTs from the southeastern tropical Indian Ocean to around the Maritime Continent, enhanced convection is expected from west of Sumatra to the southern part of Southeast Asia. In the lower troposphere, cyclonic circulation anomalies straddling the equator are expected from the central to eastern tropical Indian Ocean, and anti-cyclonic circulation anomalies straddling the equator are expected from the western to central tropical Pacific.

1. Sea surface temperature

Figure 2-1 shows predicted SSTs (contours) and related anomalies (shading) for JJA. Negative anomalies are expected in central-to-eastern parts of the equatorial Pacific. Subsurface warm waters observed in the western part are expected to migrate eastward and slightly increase SSTs in the eastern part in boreal summer. La Niña conditions are likely to continue until early boreal summer. In the tropical Indian Ocean, positive anomalies in the southeastern part and negative anomalies in the western part are expected in boreal summer.

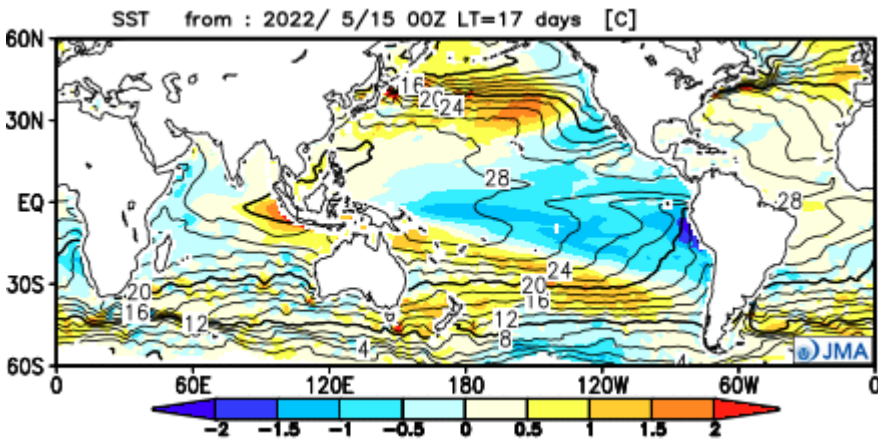


Figure 2-1 Predicted SSTs (contours) and SST anomalies (shading) for June–August 2022 (ensemble mean of 51 members)

2. Prediction for the tropics and sub-tropics

Figure 2-2 (a) shows predicted precipitation (contours) and related anomalies (shading) for JJA. In association with positive SST anomalies from the southeastern tropical Indian Ocean to around the Maritime Continent, above-normal precipitation is expected from west of Sumatra to the southern part of Southeast Asia. Below-normal precipitation is expected over the western-to-central equatorial Pacific.

Figure 2-2 (b) shows predicted velocity potential (contours) and related anomalies (shading) in the upper troposphere for JJA. In association with the precipitation anomalies detailed above, negative (i.e., large-scale

divergent) anomalies are expected from the tropical Indian Ocean to the Maritime Continent, while positive (i.e., large-scale convergent) anomalies are expected near the date line to the eastern part of the equatorial Pacific.

Figure 2-2 (c) shows predicted stream functions (contours) and related anomalies (shading) in the upper troposphere for JJA. Anti-cyclonic (i.e., positive in the Northern Hemisphere) circulation anomalies straddling the equator are expected from the tropical Atlantic to the tropical Indian Ocean, and cyclonic (i.e., negative in the Northern Hemisphere) circulation anomalies straddling the equator are expected over the central tropical Pacific.

Figure 2-2 (d) shows predicted stream functions (contours) and related anomalies (shading) in the lower troposphere for JJA. Cyclonic (i.e., negative in the Northern Hemisphere) circulation anomalies straddling the equator are expected from the central to eastern tropical Indian Ocean, and anti-cyclonic (i.e., positive in the Northern Hemisphere) circulation anomalies straddling the equator are expected from the western to central tropical Pacific.

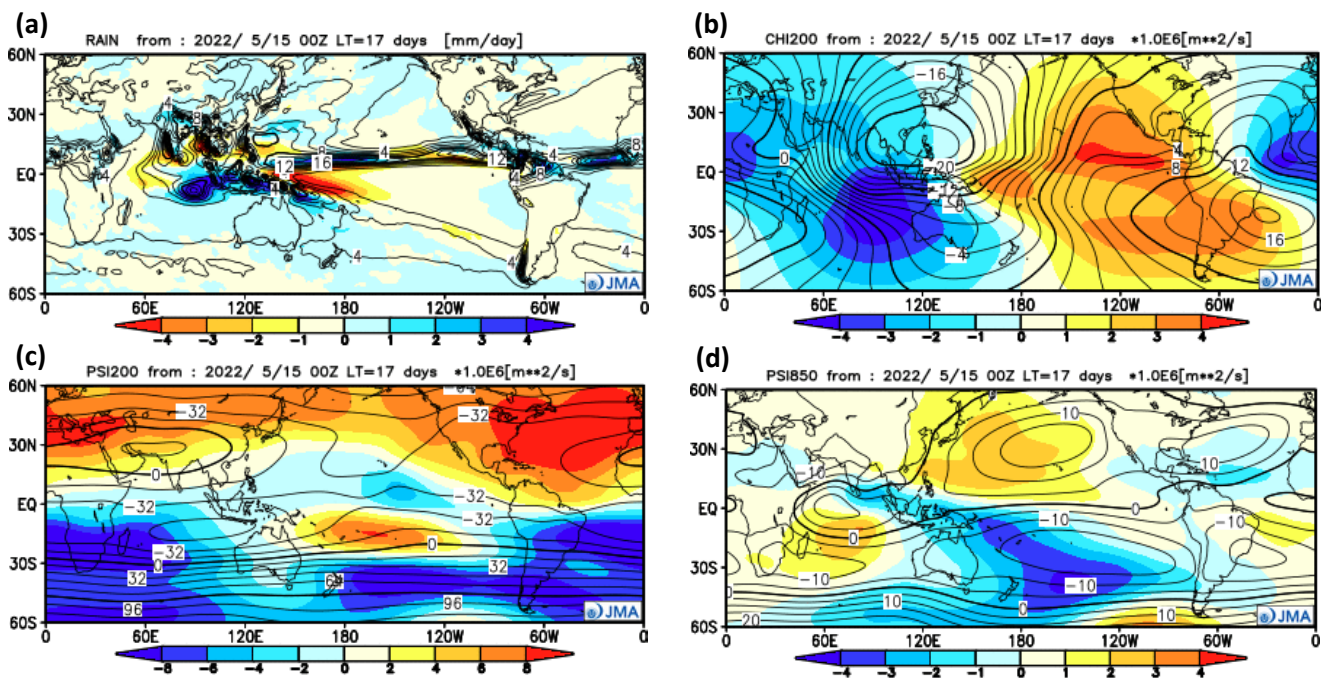


Figure 2-2 Predicted atmospheric fields over 60°N-60°S for June–August 2022 (ensemble mean of 51 members)

(a) Precipitation (contours) and anomaly (shading). The contour interval is 2 mm/day. (b) Velocity potential at 200-hPa (contours) and anomaly (shading). The contour interval is 2×10^6 m²/s. (c) Stream function at 200-hPa (contours) and anomaly (shading). The contour interval is 16×10^6 m²/s. (d) Stream function at 850-hPa (contours) and anomaly (shading). The contour interval is 5×10^6 m²/s.

3. Prediction for the mid- and high- latitudes of the Northern Hemisphere

Figure 2-3 (a) shows predicted 500-hPa geopotential heights (contours) and related anomalies (shading) for JJA. Positive anomalies are expected over the Northern Hemisphere mid-latitudes, especially to the northeast of Japan.

Figure 2-3 (b) shows predicted sea level pressure (contours) and related anomalies (shading) for JJA. Positive anomalies are expected over a wide area of the North Pacific, and negative anomalies are expected over a wide area of Eurasia and the northern part of North America.

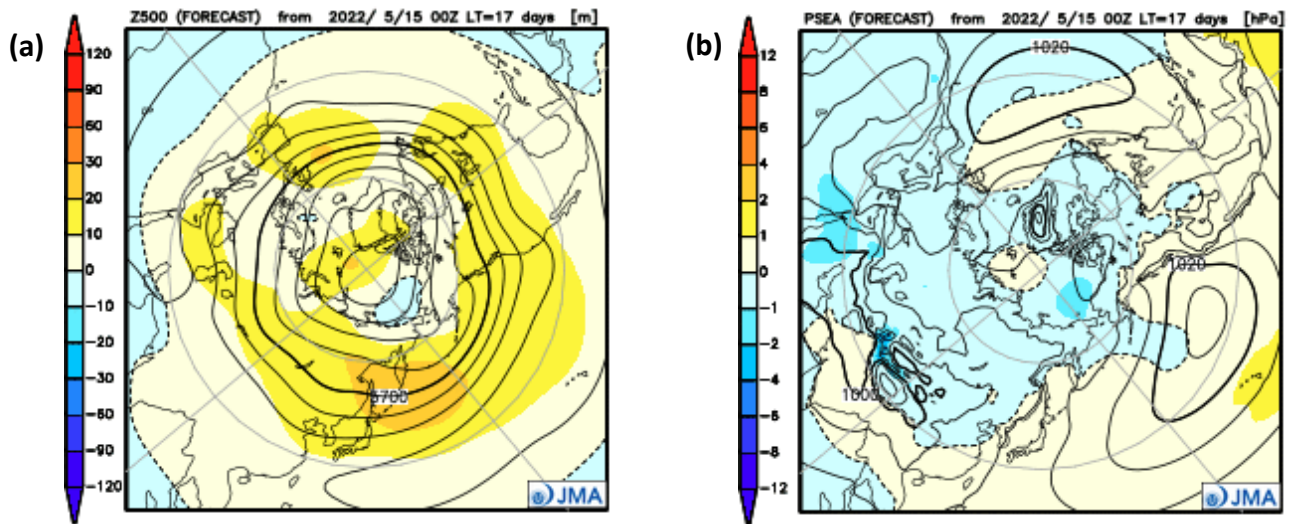


Figure 2-3 Predicted atmospheric fields in the Northern Hemisphere for June–August 2022 (ensemble mean of 51 members)
 (a) Geopotential height at 500-hPa (contours) and anomaly (shading). The contour interval is 60 m. (b) Sea level pressure (contours) and anomaly (shading). The contour interval is 4 hPa.

Note: JMA operates a seasonal Ensemble Prediction System (EPS) using the Coupled atmosphere-ocean General Circulation Model (CGCM) to make seasonal predictions beyond a one-month time range. The EPS produces perturbed initial conditions by means of a combination of the initial perturbation method and the lagged average forecasting (LAF) method. Prediction is made using 51 members from the latest 17 initial dates (3 members are used every day). Details of the prediction system and verification maps based on 30-year hindcast experiments (1991–2020) are available at <https://ds.data.jma.go.jp/tcc/tcc/products/model/>.

(SATO Hitoshi, Tokyo Climate Center)

[<<Table of contents](#) [<Top of this article](#)

Summary of the 2021/2022 Asian Winter Monsoon

This report summarizes the characteristics of the surface climate and atmospheric/oceanographic conditions related to the Asian winter monsoon for 2021/2022.

Note: The Japanese 55-year Reanalysis dataset (JRA-55; Kobayashi et al. 2015) and COBE-SST (Ishii et al. 2005) were used to analyze atmospheric circulation and sea surface temperature (SST). NOAA Interpolated Outgoing Longwave Radiation (OLR) data (Liebmann and Smith 1996) from the U.S. NOAA Physical Sciences Laboratory (PSL) (https://psl.noaa.gov/data/gridded/data.interp_OLR.html) were used to infer tropical convective activity. The base period for the normal is 1991 to 2020. The term “anomaly” as used in this report refers to deviation from the normal.

1. Surface climate conditions

In winter 2021/2022, three-month (DJF) mean temperatures were above normal in and around Central Asia and below normal over southwestern China and western Japan (Figure 3-1 (a)). Above-normal temperatures over parts of Eastern Siberia and below-normal temperatures over western Japan were seen in January and February (Figure 3-1 (c–d)), in contrast to the temperature anomaly observed in December (Figure 3-1 (b)). Temperatures were significantly below normal over most of East Asia in February (Figure 3-1 (d)), corresponding to a stronger-than-normal East Asian Winter Monsoon (EAWM). Precipitation amounts during the winter period were above normal over a wide region from South Asia to southwestern China and the southeastern part of Eastern Siberia, and were below normal from the Korean Peninsula to western Japan (Figure 3-2). Above-normal precipitation over a wide region of Southeast Asia was clearly seen in February in particular (Figure 3-2 (d)).

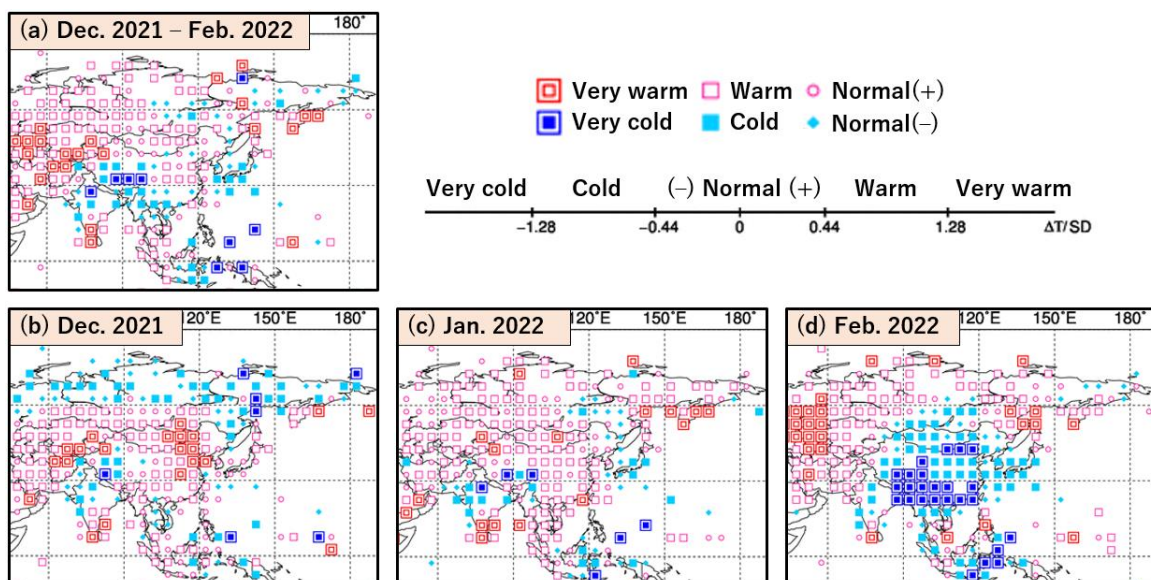


Figure 3-1 Temperature anomalies for (a) December 2021 to February 2022, (b) December 2021, (c) January 2022 and (d) February 2022

Categories are defined by the three-month/monthly mean temperature anomaly against the normal divided by its standard deviation and averaged in $5^\circ \times 5^\circ$ grid boxes. The thresholds of each category are -1.28 , -0.44 , 0 , $+0.44$ and $+1.28$. Standard deviations were calculated from 1991 – 2020 statistics. Areas over land without graphical marks are those where observation data are insufficient or where normal data are unavailable.

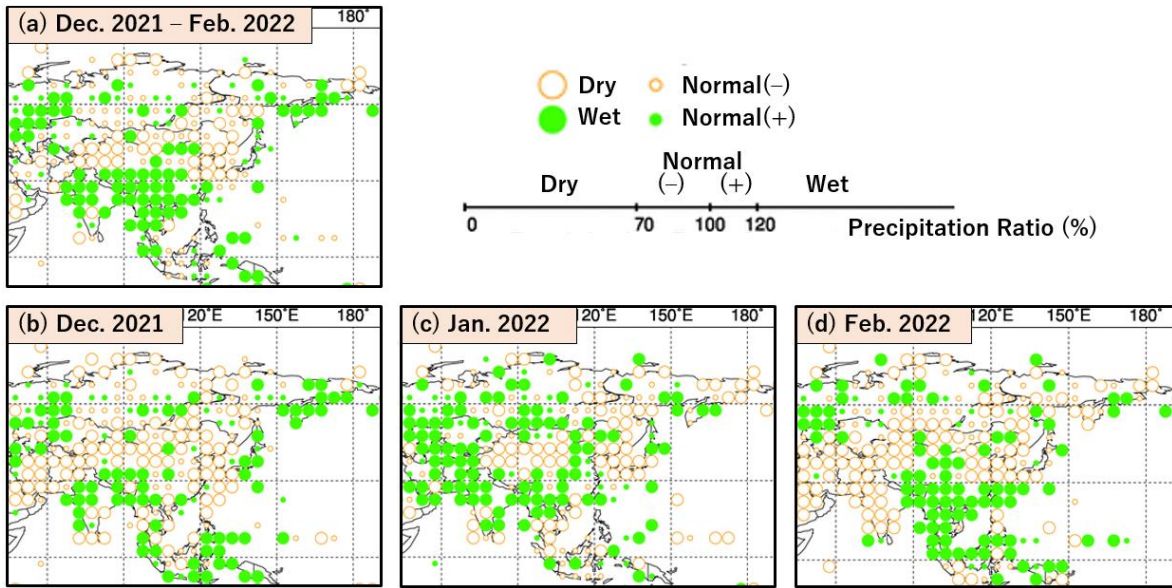


Figure 3-2 Precipitation ratio for (a) December 2021 to February 2022, (b) December 2021, (c) January 2022 and (d) February 2022

Categories are defined by the three-month/monthly precipitation ratio against the normal and averaged in 5° × 5° grid boxes. The thresholds of each category are 70, 100 and 120%. Areas over land without graphical marks are those where observation data are insufficient or where normal data are unavailable.

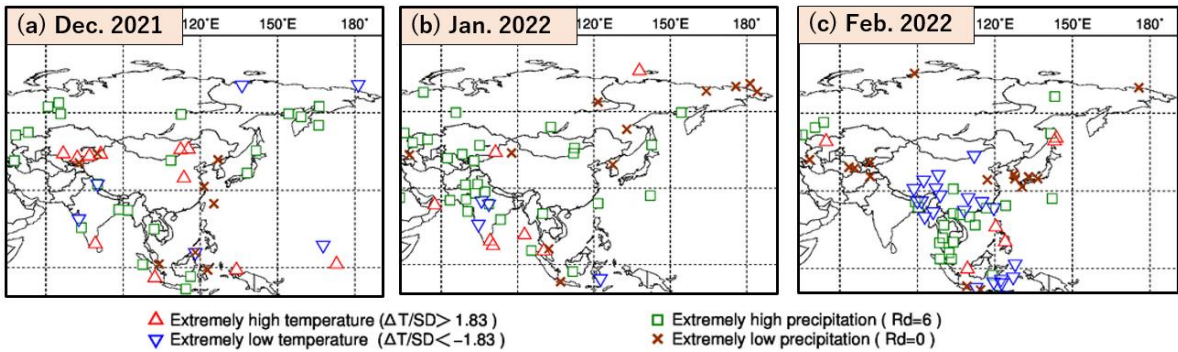


Figure 3-3 Extreme climate stations for (a) December 2021, (b) January 2022 and (c) February 2022

ΔT , SD and Rd indicate temperature anomaly, standard deviation and quintile, respectively.

Figure 3-3 plots stations where extreme climate conditions were observed during the period from December 2021 to February 2022. Extremely low temperatures were seen in and around southern China in February (Figure 3-3 (c); see also Figure 3-1 (d)). Extremely high precipitation amounts were seen in and around northwestern India in January (Figure 3-3 (b)) and on and around the Indochina Peninsula in February (Figure 3-3 (c)). Extremely low precipitation amounts were seen in and around western Japan in February (Figure 3-3 (c)).

2. Characteristic atmospheric circulation and oceanographic conditions

This section presents characteristics of atmospheric circulation and oceanographic conditions averaged for winter 2021/2022.

2.1 Conditions in the tropics

Figure 3-4 shows three-month mean SST anomalies and anomalous convective activity seen during the winter period. SSTs exhibited negative anomalies east of 170°E in the equatorial Pacific and positive anomalies over the tropical western North Pacific (Figure 3-4 (a)) in association with the La Niña event that persisted from boreal autumn 2021 onward. In the Indian Ocean, remarkably positive SST anomalies were seen in the Bay of Bengal and west of Sumatra (Figure 3-4 (a)). Convective activity inferred from OLR was enhanced from the Philippines to the seas north of New Guinea and suppressed from near the date line to the central part of the equatorial Pacific (Figure 3-4 (b)), corresponding to SST anomalies associated with the La Niña event (Figure 3-4 (a)). In the upper troposphere, large-scale divergence anomalies were dominant near the Maritime Continent, and large-scale convergence anomalies were seen from the date line to the east over the equatorial Pacific, concomitant with tropical convection (Figure 3-4 (b)). Large-scale anomalous divergence promoted northward divergent winds from the Maritime Continent to the seas south of Japan (vectors in Figure 3-4 (b)), partly contributing to a meandering of the subtropical jet stream (STJ) as described later.

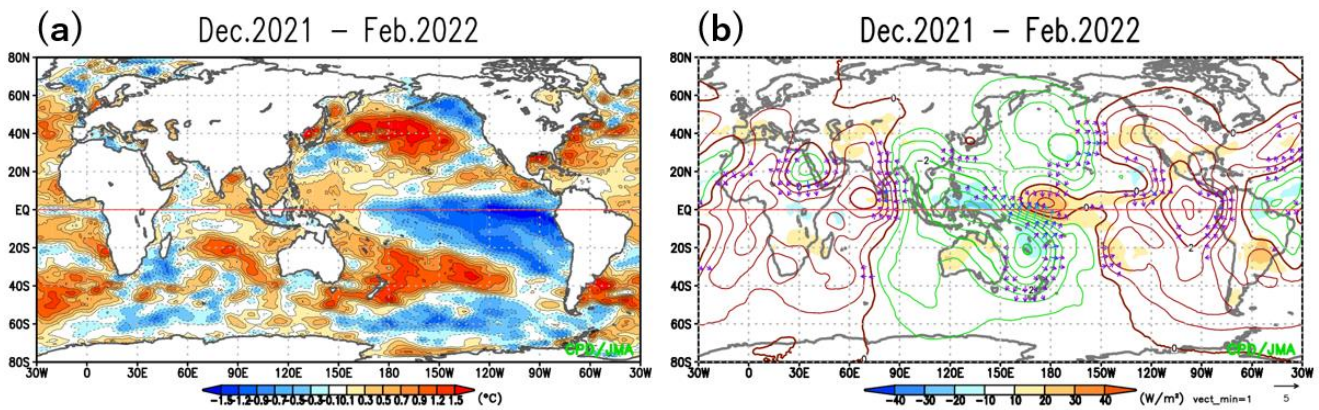


Figure 3-4 Three-month mean (a) SST anomalies and (b) anomalous convective activity in winter 2021/2022

Shading in (a) and (b) shows SST anomalies [°C] and OLR anomalies [W/m^2]. Contours and vectors in (b) indicate 200-hPa velocity potential anomalies at intervals of $0.5 \times 10^6 \text{ m}^2/s$ and divergent wind anomalies, respectively. Negative (cold color) and positive (warm color) OLR anomalies show enhanced and suppressed convective activity compared to the normal, respectively.

Figure 3-5 shows three-month mean 200-hPa and 850-hPa stream function anomalies for the winter period. In the upper troposphere, a Rossby wave train was dominant along the STJ from the eastern part of Northern Africa to the seas east of Japan. The wave train was associated with anti-cyclonic circulation anomalies over the East China Sea and cyclonic circulation anomalies near western China and to the east of Japan (Figure 3-5 (a)). The cyclonic circulation anomalies near western China, which imply a southward meandering of the STJ, correspond to below-normal temperatures and above-normal precipitation near southwestern China (Figures 3-1 (a) and 3-2 (a)). The anti-cyclonic circulation anomalies over the East China Sea may have been partly caused by northward divergent winds from the Maritime Continent, where enhanced convection was seen (Figure 3-4 (b)). This is also supported by vorticity budget analysis and the results of a numerical experiment conducted using a linear baroclinic model (Watanabe and Kimoto 2000, 2001) (not shown). In the central tropical Pacific, cyclonic circulation anomalies straddling the equator were seen in response to suppressed convection from near the date line to the eastern part of the equatorial Pacific (Figure 3-5 (a)). A great circle wave train was clearly seen from the central tropical North Pacific via North America to the North Atlantic, which is similar to behavior seen in the negative phase of the Pacific-North American (PNA) teleconnection pattern (e.g., Barnston and Livezey 1987, Horel and Wallace 1981). In the lower troposphere, anti-

cyclonic circulation anomalies straddling the equator were seen from the central to eastern tropical Pacific in response to suppressed convection from near the date line to the eastern part of the equatorial Pacific (Figure 3-5 (b)).

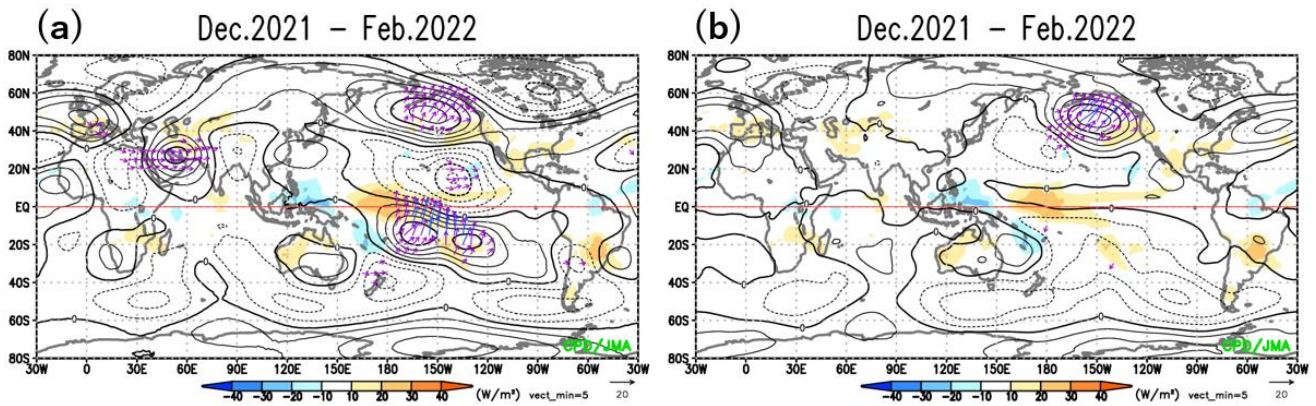


Figure 3-5 Three-month mean (a) 200-hPa and (b) 850-hPa stream function anomalies in winter 2021/2022
 Contours indicate stream function anomalies at intervals of (a) $3 \times 10^6 \text{ m}^2/\text{s}$ and (b) $1.5 \times 10^6 \text{ m}^2/\text{s}$, and shading shows OLR anomalies [W/m^2]. Vectors denote horizontal components of wave activity flux [m^2/s^2] as defined by Takaya and Nakamura (2001).

2.2 Conditions in the extratropics

Figure 3-6 shows three-month mean 500-hPa height, sea level pressure and 850-hPa temperature in the Northern Hemisphere. In the 500-hPa height field (Figure 3-6 (a)), significant positive anomalies were seen over Eastern Siberia, implying significantly frequent blocking-high formation over the region (figure not shown), and negative anomalies were seen to the south. The north-south dipole pattern of the height anomalies resembles the Western Pacific (WP) teleconnection pattern (Wallace and Gutzler 1981). The tropospheric polar vortex in the Northern Hemisphere centered from the Arctic region to northern Canada was stronger than normal. Part of the enhanced polar vortex split and moved southward to just north of Japan (contours in Figure 3-6 (a)). Wave trains associated with height anomalies were seen from Eurasia to Japan along the polar-front jet (PFJ) over northern Eurasia and the STJ over southern Eurasia. Another wave train in the Western Hemisphere from the mid-latitude North Pacific to the western North Atlantic corresponded to the negative phase of the PNA pattern (see also Figure 3-5 (a)). In the sea level pressure field (Figure 3-6 (b)), the Aleutian Low was stronger than normal and shifted southwestward from its normal position. Positive SLP anomalies from Eastern Siberia to China indicate a stronger-than-normal Siberian High. The pattern of SLP anomalies indicates a stronger-than-normal EAWM, corresponding to below-normal temperatures from southern China to mainland Japan in the lower troposphere (Figure 3-6 (c)). Lower-level temperatures, by contrast, were above normal over Siberia in association with positive 500-hPa height anomalies (Figure 3-6 (a)).

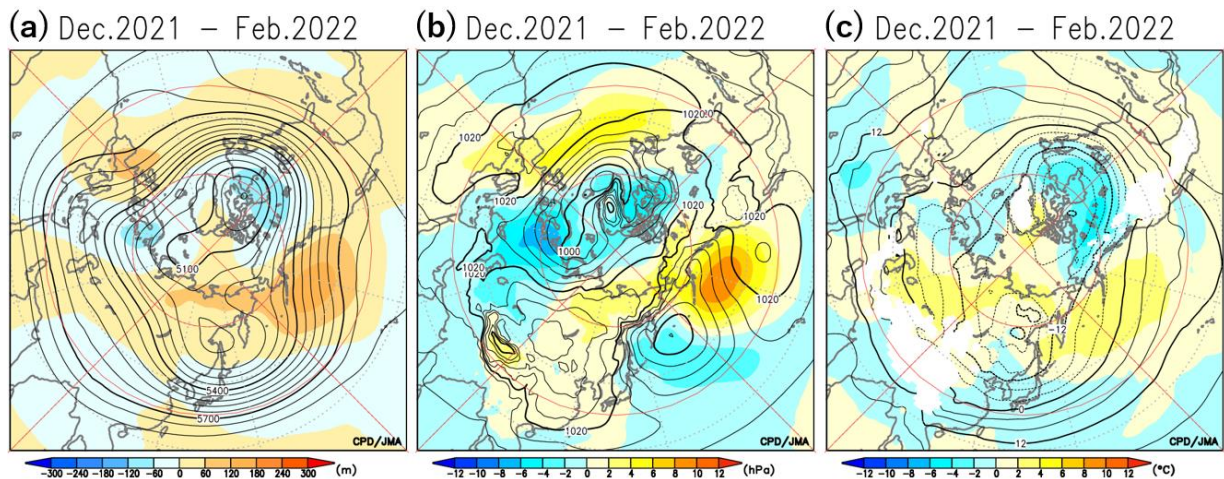


Figure 3-6 Three-month mean (a) 500-hPa height, (b) sea level pressure and (c) 850-hPa temperature in winter 2021/2022. Contour intervals are (a) 60 m, (b) 4 hPa and (c) 4 °C. Shading denotes related anomalies.

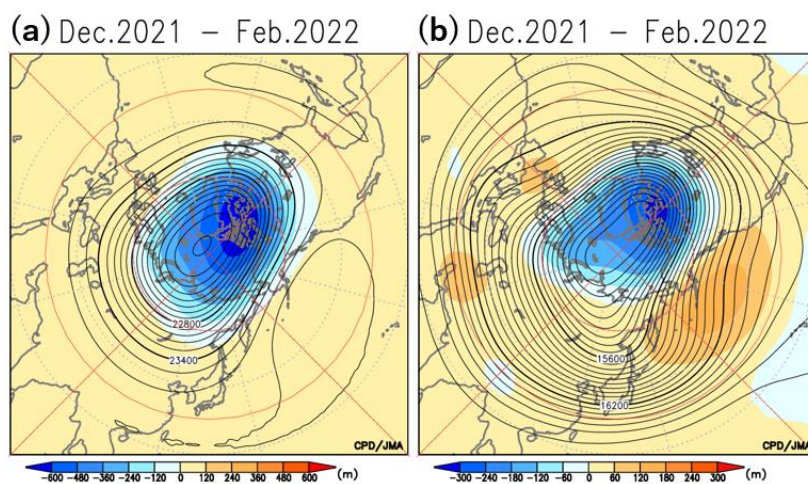


Figure 3-7 Three-month mean (a) 30-hPa and (b) 100-hPa height in winter 2021/2022. Contour intervals are (a) 120 m and (b) 60 m. Shading denotes related anomalies.

In the sea level pressure field, significant negative and positive anomalies with a north-south dipole pattern were seen over the North Atlantic, showing the positive phase of the North-Atlantic Oscillation (NAO; e.g., Hurrell 1995). The NAO in winter is known to be associated with stratospheric circulation caused by stratosphere-troposphere interaction (e.g., Ambaum and Hoskins 2002, Ineson and Scaife 2009). Figure 3-7 shows three-month mean 30-hPa and 100-hPa height in the Northern Hemisphere. Negative height anomalies at 30 hPa and 100 hPa were clearly seen from the Arctic region to northern Canada, indicating that the stratospheric polar vortex was stronger than normal and slightly shifted toward Canada during the winter period. The negative anomalies seen over northern Canada in the stratosphere correspond well with those seen in the troposphere (Figure 3-6 (a)) and near the surface (Figure 3-6 (b)), suggesting a close relationship to the positive phase of the NAO resulting from stratosphere-troposphere interaction.

(Kazuto Takemura, Tokyo Climate Center)

References

- Ambaum, M. H. P., and B. J. Hoskins, 2002: The NAO troposphere–stratosphere connection. *J. Climate*, **15**, 1969–1978.
- Barnston, A. G., and R. E. Livezey, 1987: Classification, seasonality and persistence of low-frequency atmospheric circulation patterns. *Mon. Wea. Rev.*, **115**, 1083–1126.
- Horel, J. D., and J. M. Wallace, 1981: Planetary-scale atmospheric phenomena associated with the Southern Oscillation. *Mon. Wea. Rev.*, **109**, 813–829.
- Hurrell, J. W., 1995: Decadal trends in the North Atlantic Oscillation and relationships to regional temperature and precipitation. *Science*, **269**, 676–679.
- Ineson, S., and I. I. Scaife, 2009: The role of the stratosphere in the European climate response to El Niño. *Nature Geosci.*, **2**, 32–36.
- Ishii, M., A. Shouji, S. Sugimoto, and T. Matsumoto, 2005: Objective analyses of sea-surface temperature and marine meteorological variables for the 20th century using ICOADS and the Kobe Collection. *Int. J. Climatol.*, **25**, 865–879.
- Kobayashi, S., Y. Ota, Y. Harada, A. Ebita, M. Moriya, H. Onoda, K. Onogi, H. Kamahori, C. Kobayashi, H. Endo, K. Miyaoka, and K. Takahashi, 2015: The JRA-55 Reanalysis: General specifications and basic characteristics. *J. Meteor. Soc. Japan*, **93**, 5–48.
- Liebmann, B., and C. A. Smith, 1996: Description of a complete (interpolated) outgoing longwave radiation dataset. *Bull. Amer. Meteor. Soc.*, **77**, 1275–1277.
- Takaya, K., and H. Nakamura, 2001: A formulation of a phase-independent wave-activity flux for stationary and migratory quasigeostrophic eddies on a zonally varying basic flow, *J. Atom. Sci.*, **58**, 608–627.
- Wallace, J. M., and D. S. Gutzler, 1981: Teleconnections in the geopotential height field during the Northern Hemisphere winter, *Mon. Wea. Rev.*, **109**, 784–812.
- Watanabe, M., and M. Kimoto, 2000: Atmospheric-ocean thermal coupling in the North Atlantic: A positive feedback. *Quart. J. Roy. Meteor. Soc.*, **126**, 3343–3369.
- Watanabe, M., and M. Kimoto, 2001: Corrigendum. *Quart. J. Roy. Meteor. Soc.*, **127**, 733–734.

[<<Table of contents](#) [<Top of this article](#)

TCC and WMC Tokyo co-contributions to Regional Climate Outlook Forums

WMO Regional Climate Outlook Forums (RCOFs) bring together national, regional and international climate experts on an operational basis to produce regional climate outlooks based on input from participating NMHSs, regional institutions, Regional Climate Centres (RCCs) and global producers of climate predictions. By providing a platform for countries with similar climatological characteristics to discuss related matters, these forums ensure consistency in terms of access to and interpretation of climate information.

In spring 2022, experts from TCC and the World Meteorological Centre (WMC) Tokyo gave presentations on climate outlooks and TCC activities at the following RCOFs, which were held online due to the ongoing COVID-19 pandemic.

- the 18th session of the Forum on Regional Climate Monitoring, Assessment and Prediction for Regional Association II (FOCRA II-18)
- the 22th summer session of the South Asian Climate Outlook Forum (SASCOF-22)

As part of collaborative activities between TCC and WMC Tokyo, the experts from TCC and WMC Tokyo provided summer season outlooks including probabilistic forecasts based on JMA's dynamical seasonal ensemble prediction system as well as Copernicus Climate Change Service (C3S) multi-model ensemble prediction, which the Japan Meteorological Agency (JMA) has joined in since October 2020. The presenters also covered climate monitoring and highlighted efforts to promote the use of TCC climate prediction information. These activities are intended to support the output of country-scale outlooks by National Meteorological and Hydrological Services (NMHSs), contribute to the summarization of consensus outlooks and reduce climate disaster risks in the water, agriculture and health sectors for each target area. TCC and WMC Tokyo are committed to collaboration with operational climate communities to enhance progress in forecast skill and application of climate information toward the resolution of common issues and realizing a climate-resilient world.

(TAKAHASHI Kiyotoshi, Tokyo Climate Center)

[<<Table of contents](#) [<Top of this article](#)

You can find the latest newsletter from the Japan International Cooperation Agency (JICA).

JICA Magazine

<https://jicamagazine.jica.go.jp/en/>

"JICA magazine" is a public relations magazine published by JICA. It introduces the current situations of developing countries around the world, the people who are active in the field, and the content of their activities.

Any comments or inquiry on this newsletter and/or the TCC website would be much appreciated.

Please e-mail to tcc@met.kishou.go.jp.

(Editors: NEMOTO Noboru, TAKAHASHI Kiyotoshi)

Tokyo Climate Center, Japan Meteorological Agency
3-6-9 Toranomon, Minato City, Tokyo 105-8431, Japan

TCC Website:

<https://ds.data.jma.go.jp/tcc/tcc/index.html>

[<<Table of contents](#)